2009

A cross-comparison of field, spectral, and lidar estimates of forest canopy cover

Alistair M.S. Smith
University of Idaho, alistair@uidaho.edu

Michael J. Falkowski
University of Idaho, Falk4587@uidaho.edu

Andrew T. Hudak
Rocky Mountain Research Station, ahudak@fs.fed.us

Jeffrey S. Evans
The Nature Conservancy, jeffrey_evans@tnc.org

Andrew P. Robinson
University of Melbourne, a.robinson@ms.unimelb.edu.au

See next page for additional authors

Can. J. Remote Sensing, Vol. 35, No. 5, pp. 447–459, 2009

A cross-comparison of field, spectral, and lidar estimates of forest canopy cover

Alistair M.S. Smith, Michael J. Falkowski, Andrew T. Hudak, Jeffrey S. Evans, Andrew P. Robinson, and Caiti M. Steele

Abstract. A common challenge when comparing forest canopy cover and similar metrics across different ecosystems is that there are many field- and landscape-level measurement methods. This research conducts a cross-comparison and evaluation of forest canopy cover metrics produced using unmixing of reflective spectral satellite data, light detection and ranging (lidar) data, and data collected in the field with spherical densiometers. The coincident data were collected across a ~25 000 ha mixed conifer forest in northern Idaho. The primary objective is to evaluate whether the spectral and lidar canopy cover metrics are each statistically equivalent to the field-based metrics. The secondary objective is to evaluate whether the lidar data can elucidate the sources of error observed in the spectral-based canopy cover metrics. The statistical equivalence tests indicate that spectral and field data are not equivalent (slope region of equivalence = 43%). In contrast, the lidar and field data are within the acceptable error margin of most forest inventory assessments (slope region of equivalence = 13%). The results also show that in plots where the mean lidar plot heights are near zero, each of modeled remotely sensed estimates continues to report canopy cover >21% for lidar and >30% for all investigated spectral methods using near-infrared bands. This suggests these metrics are sensitive to the presence of herbaceous vegetation, shrubs, seedlings, saplings, and other subcanopy vegetation.

Résumé. Un défi rencontré fréquemment en comparant les mesures du couvert forestier ou autres mesures semblables à travers différents écosystèmes vient du fait qu'il existe plusieurs méthodes de mesure sur le terrain ainsi qu'au niveau du paysage. Dans cette recherche, on compare et on évalue les mesures du couvert forestier réalisées à l'aide de trois approches différentes, c.-à-d. le démixage des données spectrales satellitaires, les données lidar (« light detection and ranging ») et l'acquisition de données sur le terrain avec des densitomètres sphériques. Des données simultanées ont été acquises sur l'ensemble d'une forêt mixte de conifères de ~25 000 ha dans le nord de l'Idaho. L'objectif premier est d'évaluer si les mesures du couvert à l'aide des données spectrales et lidar sont statistiquement équivalentes par rapport aux mesures sur le terrain. Le second objectif est d'évaluer si les données lidar peuvent élucider les sources d'erreur observées dans les mesures du couvert dérivées des mesures spectrales. Les tests d'équivalence statistique indiquent que les données spectrales et de terrain ne sont pas équivalentes (région d'équivalence de la pente = 43 %). Par contre, les données lidar et de terrain se situent à l'intérieur de la marge d'erreur acceptable de la plupart des évaluations d'inventaires forestiers (région d'équivalence de la pente = 13 %). Les résultats montrent également que, dans les parcelles où les hauteurs lidar moyennes sont près de zéro, chacune des estimations modélisées par télédétection continue de donner un couvert de >21 % pour le lidar et de >30 % pour toutes les méthodes spectrales analysées en utilisant les bandes du moyen infrarouge. Ceci laisse supposer que ces mesures sont sensibles à la présence de végétation herbacée, d'arbustes, de semis, de gaules ou d'autre végétation présente sous le couvert.
[Traduit par la Rédaction]

Introduction

Forest canopy cover (CC_{Forest}), which is commonly defined as a projection of the vertical profile of canopy foliage onto a horizontal plane (Fiala et al., 2006), is a useful metric for several biophysical and natural resource management applications (Hopkinson and Chasmer, 2009). These application areas include the assessment of wildlife habitat (Koy et al., 2005; Fiala et al., 2006), parameterization of fire behavior simulation models (Finney, 1998), characterization of carbon pools and sources (Chopping et al., 2008), quantification of canopy light transmission (Lieffers et al.,

Received 9 May 2009. Accepted 10 November 2009. Published on the Web at http://pubservices.nrc-cnrc.ca/cjrs on 12 April 2010.

A.M.S. Smith.[1] Forest and Rangeland Measurements Laboratory, University of Idaho, Moscow, ID 83844, USA.

M.J. Falkowski. School of Forest Resources and Environmental Science, Houghton, MI 49931, USA.

A.T. Hudak. Rocky Mountain Research Station, US Forestry Service, Moscow, ID 83844, USA.

J.S. Evans. The Nature Conservancy, Fort Collins, CO 80524-2863, USA.

A.P. Robinson. Department of Mathematics and Statistics, University of Melbourne, Melbourne Australia.

C.M. Steele. Jornada Experimental Range, USDA Agriculture Research Service, New Mexico State University, Las Cruces, NM 88003, USA.

[1]Corresponding author (e-mail: alistair@uidaho.edu).

1999), and ecosystem structure classification (Lovell et al., 2003; Fiala et al., 2006; Lee and Lucas 2007), among others (Fiala et al., 2006; Chopping et al., 2008). Furthermore, the United Nations Food and Agriculture Organization (FAO) definition of forest includes a canopy cover parameter, and therefore improvement of such estimates is of global significance, especially in areas with a high canopy cover (FAO, 2000).

One of the challenges with comparing canopy cover estimates across studies or ecosystems is the number of field- and landscape-level measurement methods that exist. As outlined in recent studies, field-based measurement of CC_{Forest} can be obtained using a wide range of equipment, including hemispherical photography, spherical densiometers, the moosehorn densitometer, point counts, stem maps, and line intercept methods (Fiala et al., 2006; Korhonen et al., 2006). An important distinction between these field methods is that hemispherical photographs and spherical densiometers integrate information from the sky hemisphere over a single point on the ground, which could be considered as a measure of *canopy closure*, whereas the other field methods measure canopy presence–absence above a spatially distributed two-dimensional (2D) sample of points on the ground, which is a measure of *canopy cover* (Jennings et al., 1999). Furthermore, light detection and ranging (lidar) data add a third dimension to the problem by including a distribution of points within a three-dimensional (3D) volume of space above the ground, perhaps making the term *canopy density* more appropriate. Clearly these different terms are confusing, especially given their slightly different interpretations, requiring a need for ease and consistency. Therefore, throughout this paper we use the term CC_{Forest} to describe each metric.

Landscape-level assessments of CC_{Forest} often rely on satellite and aircraft sensor imagery or, more recently, laser altimetry and light detection and ranging (lidar) data. From the perspective of these landscape-level remote sensing approaches, two types of canopy cover estimates are commonly derived: metrics describing the 2D horizontal extent of canopy, which is often expressed for a given cover type as a percentage of pixels (Asner et al., 2003; Falkowski et al., 2005), subpixel proportions (Pu et al., 2003; Xu et al., 2003; Sommers et al., 2009), and discrete image objects (Greenberg et al., 2005; Strand et al., 2006; 2008; Smith et al., 2008); or as 3D lidar metrics that represent the transmission of light through the canopy (Means et al., 1999; Chen et al., 2004; Hyde et al., 2005; Lefsky et al., 2005; Hopkinson and Chasmer, 2009).

A range of metrics have been proposed for lidar data to represent CC_{Forest} in forested ecosystems, including simple binary classifications of rasterized lidar data (i.e., pixel contains a canopy return or pixel does not contain a canopy return) (Chen et al., 2004) and other lidar metrics that relate to the proportion of returns penetrating the canopy (Hopkinson and Chasmer, 2009). Previous lidar studies have also evaluated the relationships between the mean and maximum lidar heights at a given plot with field-derived CC_{Forest} (Thomas et al., 2006; Hopkinson and Chasmer, 2009) to investigate the potential of modeling CC_{Forest} at landscape scales. However, Hopkinson and Chasmer (2009) observed poor relationships when using lidar-derived maximum plot heights to predict $CC_{Forest.}$ This may be due to skewed perspectives of the overall structure of a plot, especially if remnant, open-grown–isolated trees or single dominant trees are present; stronger relationships have been noted when using mean lidar plot heights (Thomas et al., 2006).

Although many studies have attempted to characterize CC_{Forest} via spectral remote sensing, few have compared the remotely derived CC_{Forest} estimates with coincident field measurements (e.g., Falkowski et al., 2005). Instead, datasets with higher spatial resolution (1–4 m pixel size) have been employed to validate estimates of CC_{Forest} derived from coarser resolution spectral data (Pu et al., 2003; Xu et al., 2003). In contrast, studies deriving CC_{Forest} from lidar data often compare lidar estimates with coincident field measurements (Magnussen and Boudewyn, 1998; Riano et al., 2004a; 2004b; Morsdorf et al., 2006; Hopkinson and Chasmer, 2009). This is largely due to the desire to augment traditional forest inventories with lidar data, which requires the collection of coincident field inventory data.

Lidar data have proven useful for estimating CC_{Forest}; however, because of logistical and financial constraints associated with acquiring lidar data across large areas, lidar-based characterizations of canopy metrics are often limited in spatial extent. Spectral remote sensing datasets (e.g., the Landsat series) have also been employed to estimate CC_{Forest}. However, the insensitivity of these spectral datasets to the 3D structure of vegetation canopies (Falkowski et al., 2005) often degrades the relationship between CC_{Forest} and metrics calculated from the spectral data (e.g., band ratios or vegetation indices). A further challenge when using spectral indices is that they will always produce poorer relationships than those produced simply using a multiple regression of the individual bands (Lawrence and Ripple, 1998). Nevertheless, the affordability and large area availability of spectral datasets still make them an attractive data source for characterizing CC_{Forest} across large spatial extents. Prior to using any spectral dataset to estimate CC_{Forest} across large spatial extents, the relationship between the remotely sensed data and three-dimensional forest structure must be quantified and understood.

In addition to conducting a spectral, lidar, and field cross-comparison of CC_{Forest}, the research presented in this paper also aims to quantify the relationship between spectral remotely sensed data and the 3D structure of forest canopies. This is primarily achieved by comparing estimates of CC_{Forest} derived from imagery obtained using the nadir bands of the Advanced Spaceborne Thermal Emission and Reflection Radiometer (ASTER) with lidar metrics describing the 3D structure of forest canopies. Understanding the magnitude and source of errors in CC_{Forest} metrics produced from ASTER imagery will enable an evaluation of the potential uncertainties within landscape- to global-level remote sensing products (e.g., LANDFIRE and FAO products) that use or produce similar metrics. This study seeks to answer the following specific questions: (1) Are CC_{Forest} estimates derived from both spectral

imagery and lidar data statistically equivalent to coincident field measurements of CC_{Forest}? (2) Can lidar metrics characterizing the 3D distribution of forest canopies be used to evaluate the source of errors in CC_{Forest} estimates derived from spectral imagery?

Methods

Study area and field measures

This study is centered on Moscow Mountain (**Figure 1**), which is located northeast of the city of Moscow, Idaho, USA (latitude 46°44′N, longitude 116°58′W). The site contains ~25 000 ha of mixed-conifer forest, with species predominately including *Pseudotsuga menziesii* (Douglas-fir), *Abies grandis* (grand fir), *Pinus ponderosa* (ponderosa pine), *Thuja plicata* (western red-cedar), *Pinus contorta* (lodgepole pine), *Larix occidentalis* (western larch), and *Picea engelmannii* (Engelmann spruce). As remarked in previous studies (Falkowski et al., 2005; 2006), this forest is an ideal location to evaluate the remote sensing of forest structure, given that it exhibits a wide variety of forest structure conditions arising from both a rich history of diverse land use management practices and topographically diverse conditions. In a previous study, 84 forest inventory plots were located via a two-stage (stratified systematic) sample design (Falkowski et al., 2005). This design sampled along a leaf area index (LAI) gradient, produced using an independent Landsat Thematic Mapper (TM) acquisition, within elevation and solar insolation strata to ensure that plots encompassed the full range of species composition and forest structure in the study area (Falkowski et al., 2005). This sampling design with the LAI gradient was previously presented and applied in other studies (e.g., Pocewicz et al., 2004) and enabled a range of canopy cover and structure conditions to be represented.

Each plot center was recorded with a Trimble ProXR global positioning system with a minimum of 150 logged positions that were subsequently differentially corrected and then averaged (accuracy ±0.8 m horizontally and ±1.1 m vertically). An intensive forest inventory was conducted at each of the 84 plots. Each plot had a fixed radius of 11.35 m, which represents a 0.04 ha (0.1 acre) plot commonly used for forest inventory assessment. Plot-level CC_{Forest} was estimated at each plot by averaging four spherical densiometer measurements collected at each corner of the forest inventory plot (north, south, east, west). Calculation of plot-level CC_{Forest} with spherical densiometers is a relatively simple field procedure. The densiometer has a convex mirror with 24 etched squares, each of which the user has to visually subdivide into four subsquares (or imagine four dots in the center of each subsquare). The user then holds the densiometer flat, away from their person at a consistent height (~1.5 m in this case), and counts the number of subsquares predominately occupied by "sky." This number is subtracted from the total number of subsquares (96) and multiplied by 1.04 to produce the measure of CC_{Forest}. The standard deviation of the four densitometer-derived canopy cover measurements across all plots varied between 0% and 47%, with an average of 17%. In this study these CC_{Forest} measures were considered the best available ground-truth dataset.

ASTER imagery acquisition and preprocessing

A level 1B (registered radiance at the sensor) ASTER image (acquired on 10 September 2002), encompassing the entire study area (**Figure 1**), was used in this study. Following Rowan and Mars (2003), who observed that the ASTER surface reflectance product (AST_07) exhibited high errors in topographically complex landscapes, the level 1B imagery was converted into top-of-atmosphere (TOA) reflectance and atmospherically corrected using the standard method of "dark body subtraction" using the minimum band pixel values as selected by the ENVI software package (RSI, Boulder, Colo.). Although the application of radiosonde data or the empirical line method of atmospheric correction would have been preferred, we applied dark body subtraction, given the retrospective nature of the image analysis and the ease of replicating this methodology and because both low atmospheric water content and clear skies were reported at the time of acquisition (Falkowski et al., 2005). We acknowledge that the use of this relatively simple atmospheric correction approach may account for increased error in the spectral data.

In this study we only used the nadir-view reflective ASTER bands. The backward-pointing oblique near-infrared band (band 3B) was not employed in this analysis. The spatial resolutions of the ASTER bands are 15 m for the visible to near-infrared bands and 30 m for the longer reflective infrared bands. In this study, all these nonthermal bands were resampled to retain the highest spatial resolution (i.e., 15 m). The ASTER sensor is onboard the TERRA satellite, which flies in a near-polar sun-synchronous orbit, with orbit parameters (apart from a 30 min flight lag time) identical to those of the Landsat-7 Enhanced Thematic Mapper (ETM) sensor (Abrams and Hook, 1998). Given the identical optics, we decided to analyze the spectral data in the same manner as that of prior Landsat spectral unmixing studies (Hudak et al., 2007; Smith et al., 2007; Lentile et al., 2009).

The ASTER bands were converted to radiance using the unit conversion coefficients from version 1 of the *ASTER user handbook* (Abrams and Hook, 1998). TOA reflectance was then calculated using a standard radiance to reflectance equation (Chander and Markham, 2003) with the ASTER mean solar exoatmospheric irradiances calculated for each ASTER band by convolving the spectral response function of each ASTER band with the world radiation center (WRC) data of the extraterrestrial solar spectral irradiance function (WRC values can be obtained online at http://staff.aist.go.jp/s.tsuchida/aster/cal/info/solar) (**Table 1**).

CC_{Forest} was estimated from the processed ASTER image via linear spectral unmixing (also termed mixture modeling). The linear spectral unmixing model is expressed by the following equation (Cochrane and Souza, 1998; Hudak et al., 2007):

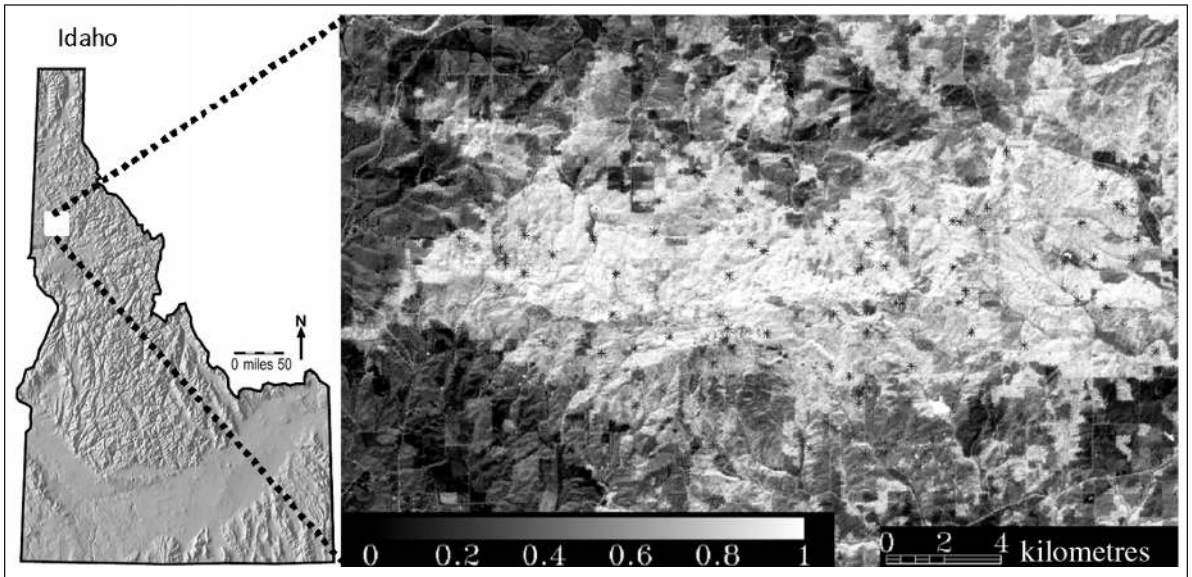

Figure 1. Forest fraction map derived from linear spectral unmixing of ASTER image acquired on 10 September 2002. The asterisks denote the location of the field plots. Image is adapted from Falkowski et al. (2005).

Table 1. ASTER specifications.

Band	Bandwidth (μm)	Spatial resolution (m)	Solar exoatmospheric irradiance of band λ, $ESUN_\lambda$[a]	
			This study[b]	Thome et al., 2001[c]
1	0.520–0.600 (green)	15	1846	1847, 1848
2	0.630–0.690 (red)	15	1556	1553, 1549
3	0.760–0.860 (NIR)	15	1120	1118, 1114
4	1.600–1.700	30	231.3	232.5, 225.4
5	2.145–2.185	30	79.8	80.3, 86.6
6	2.185–2.225	30	75.0	74.9, 81.9
7	2.235–2.285	30	68.7	69.2, 74.9
8	2.295–2.365	30	59.7	59.8, 66.5
9	2.360–2.430	30	56.9	57.3, 59.9
10	8.125–8.475	90	na	na
11	8.475–8.825	90	na	na
12	8.925–9.275	90	na	na
13	10.250–10.950	90	na	na
14	10.950–11.650	90	na	na

Note: Bands 1–9 were used in this study. na, not applicable.

[a]Calculated by interpolating the ASTER spectral response functions to 1 nm and convolving them with the 1 nm step WRC data.

[b]This information was originally presented as part of an online ASTER conversion by the authors and has been used in other studies (e.g., Yuksel et al. 2008).

[c]Calculated using spectral irradiance values derived using MODTRAN.

$$R_i = \sum_{j=1}^{n} (r_{i,j} f_j) + e_i \quad (1)$$

where R_i is the spectral reflectance for the ith band of a pixel, $r_{i,j}$ is the spectral reflectance of endmember j in band i, f_j is the fraction of endmember j in band i, and e_i is the error or unknown noise within the pixel. The subpixel proportions are then calculated by inverting Equation (1) and applying a least squares solution. The full mathematical theory can be found within the extensive linear spectral unmixing theory in the literature (Johnson et al., 1985; Smith et al., 1985; Drake and White, 1991; Drake et al., 1999; Theseira et al., 2003).

Linear spectral unmixing was performed using the four image spectral endmembers of forest, shrub, grass–meadow, and soil. Following Johnson et al. (1992), Theseira et al. (2003), and others, these endmembers were obtained by (*i*) resampling each ASTER visible to shortwave infrared band to 15 m, (*ii*) performing principal components analysis on all the resampled ASTER bands, (*iii*) producing scatterplots of the first four principal component outputs, and (*iv*) matching vertices on these scatterplots with pixels to known locations of the four cover types within the ASTER imagery.

Spectral unmixing was performed using the algorithm contained within IDL/ENVI version 4.2, with the "sum to 1" constraint applied (Drake et al., 1999). This constraint requires that proportions within a pixel add up to 1, whereas a second constraint requires that negative and proportions exceeding unity do not occur within a cover class. Although algorithms exist to enforce this second constraint under certain conditions (Shimabukuro and Smith, 1991; Settle and Drake, 1993), these approaches remain difficult to generalize (Drake et al., 1999). Following calculation of the forest cover fraction map (**Figure 1**), the pixels associated with each field plot were extracted and the mean forest fraction of those pixels within each plot was used as the linear spectral unmixing estimate of CC_{Forest}. We acknowledge that, ideally, circular ASTER pixels would be ideal for comparison with the field and lidar data given. Additionally, circular ASTER pixels would match the form of the point spread function. However, given that circular pixels either oversample the image or miss data, we used the standard square pixels for convenience.

Lidar data acquisition and preprocessing

Lidar data (1.95 m nominal post-spacing) were acquired in August 2003 across the entire Moscow Mountain study area using a Leica ALS40 system (Horizons Inc., Rapid City, S.Dak.). The lidar system operated at a wavelength of 1064 nm and was flown 2438 m above mean terrain. Although up to three returns per pulse were collected by the Leica ALS40 system, fewer than 10% of the returns were second and third returns, resulting in a majority of "ground" returns also being first returns. As such, the ground returns were classified and canopy cover was calculated without regard to return level. Following acquisition, to limit elevation errors due to slope, all returns with a scan angle >18° were removed.

The lidar data were then separated into ground and nonground returns via the multiscale curvature classification (MCC) algorithm that uses splines to remove surface curvatures not consistent with those seen in high-biomass areas. The MCC algorithm was developed for high-biomass and high-relief areas (Evans and Hudak, 2007). The root mean square errors (RMSEs) of the interpolated digital elevation model (DEM) have been previously reported in high and low canopy cover environments as 0.306 and 0.166 m, respectively (Evans and Hudak, 2007; Falkowski et al., 2008). A nearest neighbor spatial interpolation algorithm was then used to produce a 2 m DEM from the identified ground returns, and the height of each nonground return was calculated by subtracting the DEM surface from the nonground returns. The lidar canopy height data was subset to the extent of each circular 0.25 ha (0.1 acre) plot to match the plot data.

An estimate of CC_{Forest} was also derived from the lidar data. In previous lidar studies, CC_{Forest} has been defined as the percentage of "bins" containing canopy returns within a given area (Chen et al., 2004) or as the ratio of non-ground returns (i.e., canopy) to total returns (Lefsky et al., 2005; Hopkinson and Chasmer, 2009). A comparison of various methods used to define this ratio is presented in Hopkinson and Chasmer (2009). In this study, lidar-derived canopy cover, CC_L, was calculated using all the returns coincident with each forest inventory plot and defined as

$$CC_L = \frac{\text{nonground returns (above set threshold)}}{\text{total returns}} \quad (2)$$

(Means et al., 1999; Hyde et al., 2005; Lefsky et al., 2005; Morsdorf et al., 2006; Solberg et al., 2006; Hopkinson and Chasmer, 2009). Given the prior literature, the choice of the threshold above which returns are considered to be canopy has been arbitrary. For example, Morsdorf et al. (2006) define this threshold to be 1.25 m as defined by the height at which their hemispherical photographs were acquired. A threshold of 1.37 m may also be sensible, given that this is typically the height at which tree diameter (i.e., diameter at breast height (DBH)) is measured. One could also argue that the threshold should be a dynamic function defined by the transition zone between the forest understory and overstory. Higher thresholds may be warranted in single-aged plantations or similar stands that exhibit limited understory, where the threshold could conceivably be the canopy base height. However, in natural mixed-aged forests, it is likely that understory vegetation, saplings, seedlings, and shorter suppressed trees will be present. We evaluated a selection of different height thresholds (0.03, 0.50, 1.00, 1.30, 1.37, 1.40, 1.50, and 2.00 m) for calculating CC_{Forest} from the lidar data. This analysis determined a negligible variation in correlation (*r* difference of ~0.0005) between the field-densitometer-derived and lidar-derived canopy cover measures occurred when the threshold was between 1.00 and 2.00 m; therefore, we selected an intermediate threshold of 1.50 m.

Data analysis

Standard linear regression techniques were employed to evaluate the relationship between field-measured estimates of CC_{Forest} and the remotely sensed CC_{Forest} estimates (i.e., spectral- and lidar-based estimates).

Statistical equivalence tests were also employed (Wellek, 2003; Robinson and Froese, 2004) to assess whether CC_{Forest} estimates derived from the different remote sensing approaches are statistically similar (i.e., equivalent) to the field-based estimates of CC_{Forest}. Equivalence tests, which are used extensively in biostatistics (Wellek, 2003; Robinson et al.,

2005), are becoming an increasingly applied statistical tool to evaluate remote sensing data (Eitel et al., 2007; Falkowski et al., 2008; Garrity et al., 2008), presumably because remote sensing often seeks to produce remote metrics that are equivalent to field-based metrics. Statistical equivalence tests are used to test the null hypothesis of "no substantial difference" between two sample populations (H_0: the sample populations are different; H_1: the sample populations are equivalent). Following Robinson et al. (2005), we employ a regression-based equivalence test to test for intercept equality (i.e., the mean of remotely sensed CC_{Forest} estimates is equal to the mean of field-based CC_{Forest} measurements) and slope equality to 1 (i.e., if the pairwise CC_{Forest} estimates are equal, the regression will have a slope of 1). Following this process we calculate the minimum region of indifference (ε), or threshold, at which the ASTER or lidar CC_{Forest} estimates become statistically equivalent to the field-based estimates of CC_{Forest}.

Error analysis

In an attempt to assess whether noncanopy forest components were negatively influencing the CC_{Forest} estimates, regressions were performed to predict CC_{Forest} from the spectral information provided via the ASTER sensor (i.e., each band as well as common vegetation indices). These predictions, and the spectrally unmixed and lidar-derived CC_{Forest} estimates, were then related to the mean lidar height at each forest inventory plot via regression. This analysis should provide a detailed understanding of how subcanopy vegetation components influence estimates of CC_{Forest} derived via the remotely sensed data.

Results

Comparison of CC_{Forest} metrics

CC_{Forest} estimates derived from linear spectral unmixing (x_1) were linearly related to field-derived (y) estimates ($y = 1.222x_1 - 1.112$, $r^2 = 0.56$, RMSE = 22.7%) and exhibited a slight positive bias (3.3%) (**Figure 2A**). In contrast, the relationship between lidar-derived canopy cover (x_2) and field-measured canopy cover (**Figure 2B**) was much stronger and more linear ($y = 1.006x_2 + 0.047$, $r^2 = 0.78$, RMSE = 16.1%). However, there was a large negative bias (–11%).

The equivalence testing analysis indicates that the mean spectral-based canopy cover and mean field-based canopy cover estimates are statistically equivalent at the 9% equivalence level (i.e., reject the null hypothesis of intercept inequality when the rejection region (ε) is >9%). However, the slope equivalence test indicates that the pairwise canopy cover estimates are not statistically equivalent until the rejection region is greater than 43% (i.e., reject the null hypotheses of both slope and intercept inequality when the rejection region (ε) is >43%). In terms of lidar-derived canopy cover, the region of equivalence for the means and slope are both 13% (i.e., reject the null hypotheses of both slope and intercept inequality when the rejection region (ε) is >13%).

Figure 2 provides a graphical representation of the equivalence test results with a ±15% region of indifference. In terms of the spectral data (**Figure 2A**), the equivalence plot confirms that the mean of the spectral canopy cover estimates is equivalent to the mean field canopy cover estimates (i.e., the grey error bar is within the grey polygon); however, the pairwise estimates are not equivalent (i.e., the black error bar is not contained by the broken grey lines). The smooth curve fitted to the data shows that the spectral data are failing to capture the extremes. Specifically, the top quintile of the field measures occupies the top 50% of the spectral responses, and the bottom quintile of the field measures occupies the bottom 50% of the spectral responses. Also note the wide variability of the points around the fitted line (**Figure 2A**). In terms of the lidar data, the equivalence plot (**Figure 2B**) confirms that the mean and pairwise lidar canopy cover estimates are equivalent to the field canopy cover estimates (i.e., the grey error bar is within the grey polygon, and the black error bar is completely contained by the broken grey lines). The smooth curve fitted to the data shows that the lidar data are again failing to capture the extremes and that there is fairly wide variability of the points around the fitted line. Overall, however, the lidar data provide much better estimates of canopy cover than the spectral data.

Error analysis of CC_{Forest} predictions

The modeled estimates of CC_{Forest} were calculated using each of the regression equations, and the resultant values were compared with the mean lidar plot height (**Table 2**). Lidar-derived CC_{Forest} (CC_L) estimates exhibit the strongest relationship ($r^2 = 0.78$) and lowest error (RMSE = 16.1%) when regressed with field-measured CC_{Forest}, and the CC_{Forest} estimate derived via linear spectral unmixing (LSUM CC) displays a much weaker relationship ($r^2 = 0.56$) and 6.3% higher error (RMSE = 22.7%). In terms of spectral reflectance and (or) emission, most individual ASTER bands are strongly related to field-measured CC_{Forest} ($r^2 = 0.68$–0.75) and display errors of less than 18.4%. However, the relationship between field-measured CC_{Forest} and near-infrared reflectance as measured by the ASTER sensor is very weak ($r^2 = 0.09$) and contains a relatively large amount of error (RMSE = 32.4%). The relationship between field-measured CC_{Forest} and vegetation indices incorporating near-infrared reflectance is weaker ($r^2 \leq 0.65$) and has larger error (RMSE ≥ 18.9%) when compared with the green–red vegetation index (GRVI) ($r^2 = 0.76$, RMSE = 16.7%), which does not incorporate near-infrared reflectance.

Comparing each of the CC_{Forest} metrics to the mean plot height (as measured by the lidar data) demonstrates that in plots where the mean lidar plot height is near zero each of the modeled remotely sensed estimates continues to report canopy covers of greater than 21% (**Figure 3**; **Table 2**; height of y intercept (%)). Specifically, the lidar-derived CC_{Forest} estimate (CC_L) displays an intercept of 21% when regressed with mean

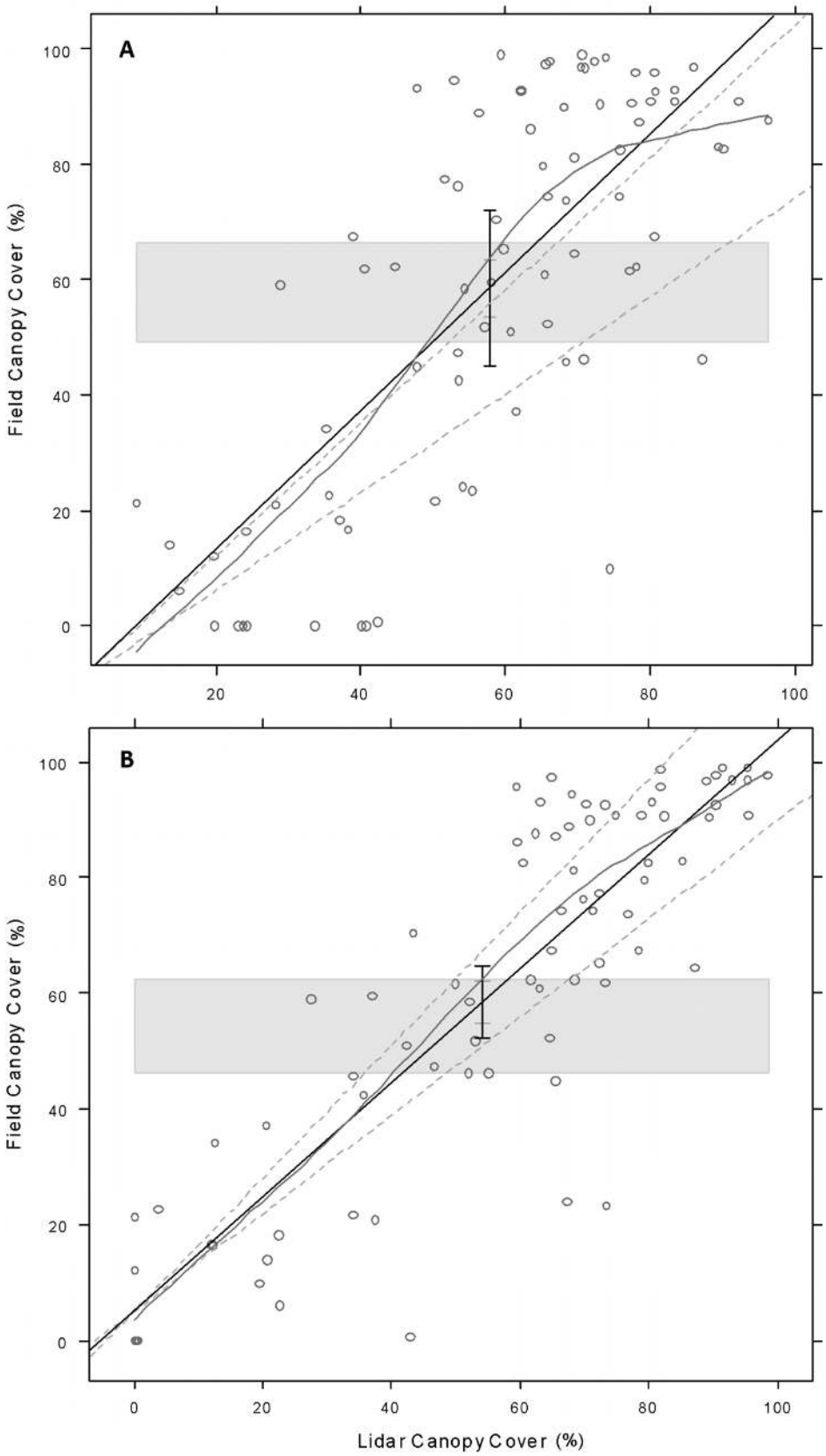

Figure 2. Canopy cover equivalence tests (ε = 15%) between each remote methodology and the field-collected data. (A) represents the spectral unmixing and field comparison, and (B) represents the lidar and field comparison.

Table 2. CC_{Forest} regression models with coefficients and model fit statistics.

Model	*p*	r^2	RMSE (%)	Height of *y* intercept (%)
1.006(CC_L) + 0.047	0.000	0.78	16.1	21
1.222(LSUM CC) – 1.112	0.000	0.56	22.7	38
–6.02b1 + 223.58[a]	0.000	0.71	18.3	31
–4.86b2 + 144.32[a]	0.000	0.75	16.9	30
–1.54b3 + 126.27[a]	0.006	0.09	32.4	53
–5.51b4 + 133.61	0.000	0.71	18.4	30
–8.76b5 + 144.03	0.000	0.68	19.3	32
–8.01b6 + 136.24	0.000	0.72	17.9	30
–9.57b7 + 142.22	0.000	0.72	17.9	30
–12.39b8 + 136.47	0.000	0.72	17.8	30
–20.07b9 + 167.66	0.000	0.71	18.2	30
278.65NDVI – 96.36[a]	0.000	0.69	18.9	35
27.92SR – 45.77[a]	0.000	0.65	20.1	36
375.51GRVI + 2.29[a]	0.000	0.76	16.7	30

Note: All regressions are significant at the 0.99 level. Field-measured CC_{Forest} is the dependent variable. b1–b9, bands 1–9; CC_L, lidar derived CC_L (= (no. of canopy returns)/(total no. of returns)); GRVI, green–red vegetation index (= (green – red)/(green + red)); height of *y* intercept, *y* intercept determined for each modeled estimate of CC_{Forest} when plotted against the mean lidar plot height; LSUM CC, fraction canopy cover from linear spectral unmixing; NDVI, normalized difference vegetation index (= (NIR – red)/(NIR + red)); SR, simple ratio (= NIR/red).

[a]Regression results first presented in Falkowski et al. (2005).

lidar height, and the spectrally unmixed estimate (LSUM CC) has an intercept of 38%. The individual ASTER bands and associated vegetation indices all display *y* intercepts greater than or equal to 30%, with the near-infrared band displaying the highest *y* intercept (53%).

Comparison of the green, red, and near-infrared ASTER reflectance bands with the lidar mean plot height demonstrates that, although a reducing trend is apparent, the near-infrared band is relatively insensitive to changes in mean lidar plot height (**Figure 3F**). Although both the green and red bands produce a good reducing trend (**Figures 3D**, **3E**), analysis shows that they are highly correlated and account for 97% of the same variability, limiting their combined usage in modeling canopy cover.

Discussion

Comparison of CC_{Forest} metrics

The differences between the cross-comparisons of lidar and spectral measures of cover and the field-based assessment can in part be attributed to how the different metrics are defined. In terms of similarity, the densiometer and lidar estimates of CC_{Forest} essentially measure light transmission through the forest canopy. For example, lidar CC_{Forest} estimates provide a measure of photon pulse transmission through the forest canopy (including leaves and associated woody material), and densiometers provide a metric of the transmission of sunlight through the forest canopy (also including leaves and associated woody material) from a hemispherical perspective. Conversely, liner spectral unmixing only provides a metric of the amount of light reflected by photosynthesizing vegetation (i.e., including green vegetation only; woody material is excluded). Furthermore, since both lidar and field densiometer metrics incorporate height thresholds (e.g., densiometer height above ground and lidar canopy threshold), such measurements are not typically influenced by understory vegetation. However, the spectrally unmixed CC_{Forest} estimates will be influenced by the presence of photosynthesizing understory vegetation, especially when overstory canopy cover is low (i.e., understory vegetation will not be occluded by the overstory canopy components). According to **Figure 2A**, this is indeed the case; there are a series of observations reporting field-measured CC_{Forest} of 0%, with spectrally unmixed estimates ranging between 20% and 40%. Since the spectrally unmixed estimates of CC_{Forest} are indeed influenced by the forest understory, such estimates are expected to be less similar to those produced using lidar and the field densiometers.

Differences could also arise from the effective view angles from which the light transmission metrics are evaluated. For example, the lidar data were acquired using a sensor field of view of less than 18° from nadir, whereas the field densiometers use a hemispherical view. A further source of error in the analysis of the ASTER data could arise from the geolocation accuracy of the ASTER pixels with respect to the plot location. Given that the field densitometer measurements were acquired at the plot corners, the field measure is assumed to represent a larger area than the 11.35 m radius circle about the plot center. As the ASTER user guide reports the geolocation accuracy as <15 m (Abrams and Hook, 1998), this error, although potentially present, may be reduced. Differences could also arise between the ASTER and lidar assessments of CC_{Forest} given the growth of the vegetation between the acquisitions.

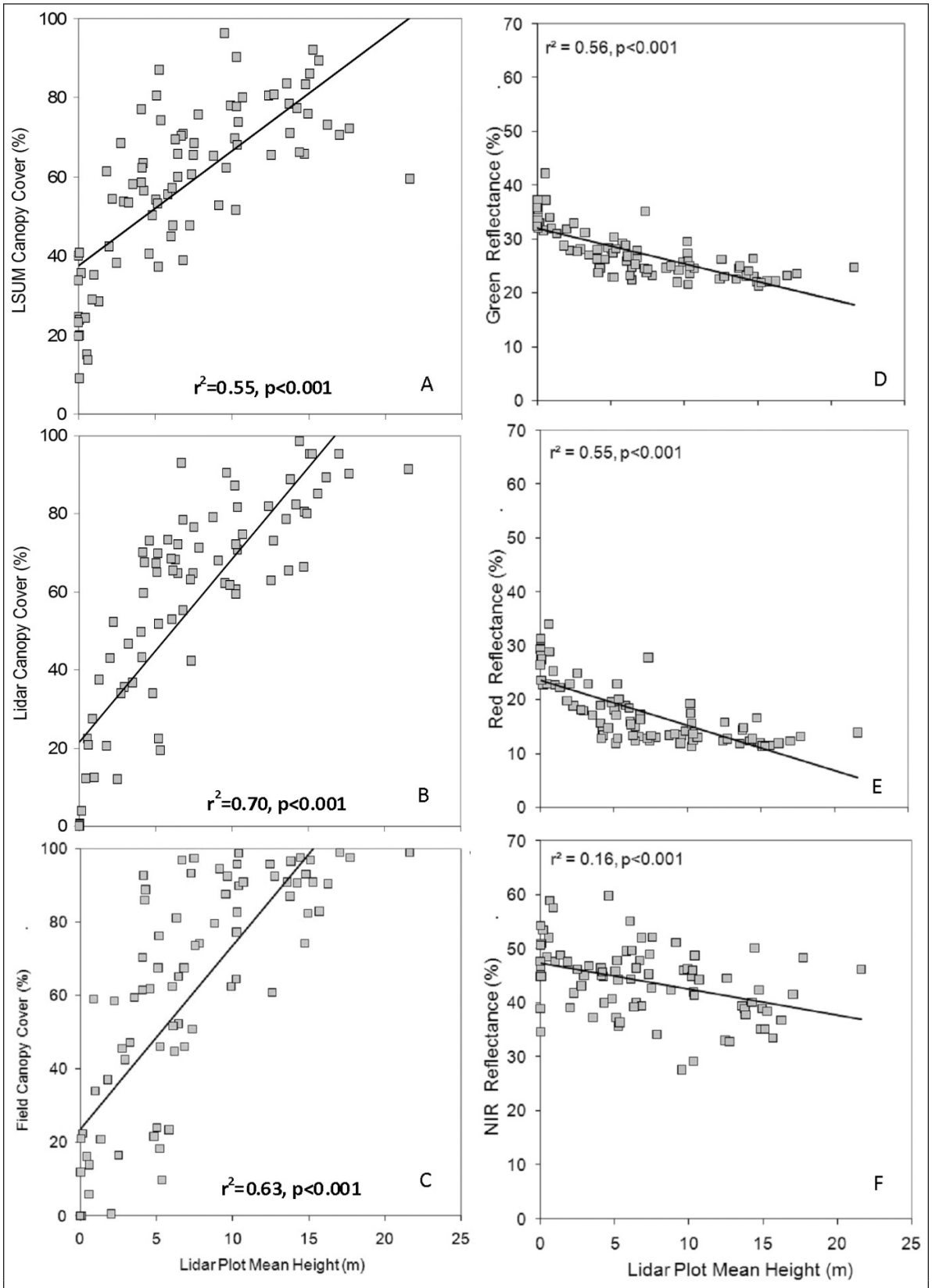

Figure 3. Comparison of the plot mean heights from the lidar data and the spectral (A), lidar (B), and field estimates (C) of percent canopy cover. (D–F) Comparison of plot mean height with reflectance of green (D), red (E), and near-infrared (F) ASTER bands.

In terms of the lidar-based CC_{Forest} estimates, **Figure 2B** exhibits a large variability of lidar estimates (60%–100%) where the field measurements indicate nearly 100% cover. This variability is likely due to the different effective resolving powers of the lidar sensor and field densiometer. CC_{Forest} is calculated from the densiometer by a human user, who must visually determine if a forest canopy component is present with each of the individual squares on the instrument. Since the presence of forest canopy is determined in a binary manner (i.e., "yes" there is canopy in the quarter of the individual densiometer square, or "no" there is not) rather than via a percent cover in each square (e.g., 50% of the individual densiometer square contains forest canopy), the densiometers may overestimate CC_{Forest}, especially when canopy cover approaches 100%. In contrast, lidar data have a much higher resolving power than spherical densiometers, and estimating CC_{Forest} via lidar data is much less subjective. As a result, as is often observed in height determination studies (Anderson et al., 2005), lidar data may indeed provide more accurate measurements of canopy cover as compared with field-based assessments.

Error analysis of CC_{Forest} predictions

The results presented in **Table 2** demonstrate that, although relationships between CC_{Forest} and lidar data are the strongest and have the lowest error rates, spectral-based predictions are fairly similar in terms of relationship strength and error rate. One caveat to this statement is the fact that the relationship between CC_{Forest} and the near-infrared reflectance is extremely weak (r^2 = 0.09) and has a high degree of error (RMSE = 32.4%). Indeed, previous studies have made similar observations when predicting CC_{Forest} from spectral data, attributing the weak relationship between CC_{Forest} and the near-infrared reflectance to the presence of senesced understory at the time of image acquisition (Xu et al., 2003; Falkowski et al., 2005). Since spectral-based estimates of CC_{Forest} are comparable to the lidar-based estimates, satellite sensors may indeed provide an efficient, accurate means to estimate CC_{Forest} across very large spatial extents.

Comparing CC_{Forest} estimates with the mean lidar plot height reveals that each remotely sensed estimate reports forest canopy cover when the mean lidar height approaches zero (**Figure 3**). These results suggest that noncanopy vegetation components are influencing CC_{Forest} estimates derived from the remote sensing data. The fact that both the field and lidar data tend to report CC_{Forest} of 21% when mean plot height is zero may suggest that the lidar mean height metric may be oversensitive to canopy vegetation in sparse, open canopy forests (e.g., forests that are characterized by open canopies and dispersed trees). These results are a considerable improvement over studies investigating the prediction of canopy cover from maximum canopy height (Hopkinson and Chasmer, 2009) and are in agreement with the prior study of Thomas et al. (2006), who observed that mean heights were good predictors of crown closure when using either low-density (r^2 = 0.61, RMSE = 40%) or high-density (r^2 = 0.75, RMSE = 32%) lidar data.

Alternatively, and perhaps more likely, this is a result of known errors associated with field-based methods used to measure forest canopy cover. Specifically, spherical densiometer measurements in young open canopy forests will exhibit a higher variability as compared with measurements taken in older open canopy or closed canopy forests (Fiala et al., 2006). This is because the probability of detecting low-stature trees with a densiometer in open canopy forests is lower than in forests with other types of canopy structure (Fiala et al., 2006). Low-stature, open canopy forests will likely have a mean lidar plot height near zero, despite the presence of a few short, well-dispersed trees in the forest canopy. Although the mean lidar height is near zero in such situations, the low-stature, dispersed trees would indeed be incorporated into the canopy cover calculation. This further demonstrates that lidar-based estimates of CC_{Forest} may be more accurate than field-based estimates, especially in forest with open canopy structure.

The linear relationships between CC_{Forest} estimates derived from the ASTER spectral metrics and the mean lidar height display intercepts >30%, indicating that the spectral estimates are sensitive to subcanopy vegetation components (**Table 2**). Of particular concern is the near-infrared band (b3), which estimates a canopy cover of 53% when mean lidar height approaches zero. This insensitivity to the understory is emphasized by the minimal variation in near-infrared reflectance with changes in mean lidar plot height. This is presumably due to the generally high near-infrared reflectance of understory vegetation, regardless of vegetation type or degree of senescence (Elvidge, 1990).

Conclusions

The comparison of lidar-based canopy cover to a field-based metric agrees with comparable lidar canopy cover studies (Morsdorf et al., 2006; Hopkinson and Chasmer, 2009) and supports the utility of lidar in the development of landscape-scale estimates of forest canopy cover. The results presented herein and in previous studies indicate that the lidar metric of forest canopy cover (CC_{Forest}) accounts for approximately 78% of the variability in field-based canopy cover metrics (**Table 2**). The unaccounted for 22% is likely due to the challenges identified earlier in this study and elsewhere regarding sensor limitations or plots that are shrub dominated, exhibit a high degree of ladder fuels, or have canopy gaps and larger openings (Hopkinson and Chasmer, 2009). A further source of error when comparing lidar metrics with the field data could have arisen from the highly variable spherical densiometer method used in this study. Future research is clearly warranted to evaluate the positioning of the densiometer measurements when evaluating plot canopy assessments.

Based on the results of this study, it is clear that CC_{Forest} predictions incorporating near-infrared reflectance could

grossly overestimate CC_{Forest} in open canopy forests when a large amount of understory vegetation is present. These results suggest that CC_{Forest} estimates that use spectral datasets should avoid using bands with near-infrared wavelengths. Given the widespread implications of this finding to existing landscape-scale data products, further research is clearly warranted to reassess this conclusion in other forest types. The results of the canopy cover and mean plot height regressions suggest that, after accounting for the bias due to the understory, potential exists in these mixed conifer forests to form predictive relationships between plot-based mean tree height and the remote sensing derived canopy cover. A similar methodology should be attempted in a hardwood forest to evaluate the utility of lidar mean height for the prediction of CC_{Forest} in those forest types.

Acknowledgements

Funding for this project was in part provided by the Forest Public Access Resource Center (ForestPARC), a part of the Upper Midwest Aerospace Consortium (UMAC), which receives funding from the National Aeronautics and Space Administration (NASA). This work was in part supported by the National Science Foundation (NSF) Idaho EPSCoR Program and by the NSF under award number EPS-0814387. The authors also acknowledge partial funding for this work from the following additional sources: Raytheon (NASA); the USDA Forest Service Rocky Mountain Research Station; and Agenda 2020, a joint effort of the US Department of Agriculture Forest Service Research and Development and the American Forest and Paper Association. Research partners included Bennett Lumber Products, Inc. and Potlatch Forest Holdings, Inc. Tessa Jones and Jennifer Clawson assisted in the field.

References

Abrams, M., and Hook, S. 1998. *ASTER user handbook, version 1*. NASA Jet Propulsion Laboratory, Pasadena, Calif.

Anderson, H-E., McGaughey, R.J., and Reutebuch, S.E. 2005. Estimating forest canopy fuel parameters using LIDAR data. *Remote Sensing of Environment*, Vol. 94, pp. 441–449.

Asner, G.P., Archer, S., Hughes, R.F., Ansley, R.J., and Wessman, C.A. 2003. Net change in regional woody vegetation cover and carbon storage in Texas Drylands, 1937–1999. *Global Change Biology*, Vol. 9, pp. 316–335.

Chander, G., and Markham, B. 2003. Revised Landsat-5 TM radiometric calibration procedures and post-calibration dynamic ranges. *IEEE Transactions on Geoscience and Remote Sensing*, Vol. 41, No. 11, pp. 2674–2677.

Chen, X., Vierling, L., Rowell, E., and DeFelice, T. 2004. Using lidar and effective LAI data to evaluate IKONOS and Landsat 7 ETM+ vegetation cover estimates in a ponderosa pine forest. *Remote Sensing of Environment*, Vol. 91, No. 1, pp. 14–26.

Chopping, M., Moisen, G.G., Su, L., Lalibrete, A., Rango, A., Martonchik, J., and Peter, D.P.C. 2008. Large area mapping of southwestern forest crown cover, canopy height, and biomass using the NASA Multiangle Imaging Spectro-Radiometer. *Remote Sensing of Environment*, Vol. 112, pp. 2051–2063.

Cochrane, M.A., and Souza, C.M. 1998. Linear mixture model classification of burned forests in the Eastern Amazon. *International Journal of Remote Sensing*, Vol. 19, pp. 3433–3440.

Drake, N.A., and White, K. 1991. Linear mixture modelling of Landsat Thematic Mapper data for mapping the distribution and abundance of gypsum in the Tunisian Southern Atlas. In *Spatial Data 2000: Proceedings of a Joint Conference of the Photogrammetric Society, the Remote Sensing Society, and the American Society for Photogrammetry and Remote Sensing*, 17–20 September 1991, Christ Church, Oxford. Edited by I. Dowman. University College, London, UK. pp. 168–177.

Drake, N.A., Mackin, S., and Settle, J.J. 1999. Mapping vegetation, soils, and geology in semiarid shrublands using spectral matching and mixture modeling of SWIR AVIRIS imagery. *Remote Sensing of Environment*, Vol. 68, pp. 12–25.

Eitel, J.U.H., Long, D., Gessler, P.E., and Smith, A.M.S. 2007. Using in-situ spectroradiometry to evaluate new RapidEye satellite data for prediction of wheat nitrogen status. *International Journal of Remote Sensing*, Vol. 28, No. 18, pp. 4183–4190.

Elvidge, C.D. 1990. Visible and near infrared reflectance characteristics of dry plant materials. *International Journal of Remote Sensing*, Vol. 11, pp. 1775–1795.

Evans, J.S., and Hudak, A.T. 2007. A multiscale curvature algorithm for classifying discrete return lidar in forested environments. *IEEE Transactions on Geoscience and Remote Sensing*, Vol. 45, No. 4, pp. 1029–1038.

Falkowski, M.J., Gessler, P.E., Morgan, P., Hudak, A.T., and Smith, A.M.S. 2005. Evaluating ASTER satellite imagery and gradient modeling for mapping and characterizing wildland fire fuels. *Forest Ecology and Management*, Vol. 217, pp. 129–146.

Falkowski, M.J., Smith, A.M.S., Hudak, A.T., Gessler, P.E., Vierling, L.A., and Crookston, N.L. 2006. Automated estimation of individual conifer tree height and crown diameter via two-dimensional spatial wavelet analysis of lidar data. *Canadian Journal of Remote Sensing*, Vol. 32, No. 2, pp. 153–161.

Falkowski, M.J., Smith, A.M.S., Gessler, P.E., Hudak, A.T., Vierling, L.A., and Evans, J.S. 2008. The influence of conifer forest canopy cover on the accuracy of two individual tree measurement algorithms using lidar data. *Canadian Journal of Remote Sensing*, Vol. 34, No. S2, pp. S338–S350.

FAO. 2000. *FRA 2000: On definitions of forest and forest change*. Forest Resource Assessment. UN Food and Agricultural Organization (FAO), Rome. Working Paper 33. 14 pp.

Fiala, A.C.S., Garman, S.L., and Gray, A.N. 2006. Comparison of five canopy cover estimation techniques in the western Oregon Cascades. *Forest Ecology and Management*, Vol. 232, pp. 188–197.

Finney, M.A. 1998. *FARSITE: fire area simulator-model development and evaluation*. Rocky Mountain Research Station, US Department of Agriculture, Forest Service, Ogden, Utah. Research Paper RMRS-RP-4. 47 pp.

Garrity, S.R., Vierling, L.A., Smith, A.M.S., Falkowski, M.J., and Hann, D.B. 2008. Automatic detection of shrub location, crown area, and cover using spatial wavelet analysis and aerial photography. *Canadian Journal of Remote Sensing*, Vol. 34, No. S2, pp. S376–S384.

Greenberg, J.A., Dobrowski, S.Z., and Ustin, S.L. 2005. Shadow allometry: estimating tree structural parameters using hyperspatial image analysis. *Remote Sensing of Environment*, Vol. 97, pp. 15–25.

Hopkinson, C., and Chasmer, L. 2009. Testing lidar models of fractional cover across multiple forest ecozones. *Remote Sensing of Environment*, Vol. 113, pp. 275–288.

Hudak, A.T., Morgan, P., Bobbitt, M.J., Smith, A.M.S., Lewis, S.A., Lentile, L.B., Robichaud, P.R., Clark, J.T., and McKinley, R.A. 2007. The relationship of multispectral satellite imagery to immediate fire effects. *Journal of Fire Ecology*, Vol. 3, No. 1, pp. 64–90.

Hyde, P., Dubayah, R., Peterson, B., Blair, J.B., Hofton, M., Hunsaker, C., Knox, R., and Walker, W. 2005. Mapping forest structure for wildlife habitat analysis using waveform lidar: validation of montane ecosystems. *Remote Sensing of Environment*, Vol. 96, pp. 427–437.

Jennings, S.B., Brown, N.D., and Sheil, D. 1999. Assessing forest canopies and understorey illumination: canopy closure, canopy cover and other measures. *Forestry*, Vol. 72, No. 1, pp. 59–73.

Johnson, P.E., Smith, M.O., and Adams, J.B. 1985. Quantitative analysis of planetary reflectance spectra with principal components analysis. *Journal of Geophysical Research*, Vol. 90, pp. C805–C810.

Johnson, P.E., Smith, M.O., and Adams, J.B. 1992. Simple algorithms for remote determination of mineral abundances and particles sizes from reflectance spectra. *Journal of Geophysical Research*, Vol. 97, No. E2, pp. 2649–2657.

Korhonen, L., Korhonen, E.T., Rautianen, M., and Stenberg, P. 2006. Estimation of forest canopy cover: a comparison of field measurement techniques. *Silva Fennica*, Vol. 40, No. 4, pp. 577–588.

Koy, K., McShea, W.J., Leimgruber, P., Haack, B.N., and Aung, M. 2005. Percentage canopy cover — using Landsat imagery to delineate habitat for Myanmar's endangered Eld's deer (*Cervus eldi*). *Animal Conservation*, Vol. 8, No. 3, pp. 289–296. doi:10.1017/S1367943005002209.

Lawrence, R.L., and Ripple, W.J. 1998. Comparison among vegetation indices and bandwise regression in a highly disturbed, heterogeneous landscape: Mount St. Helens, Washington. *Remote Sensing of Environment*, Vol. 64, pp. 91–102.

Lee, A.C., and Lucas, R.M. 2007. A lidar-derived canopy density model for tree stem and crown mapping in Australian forests. *Remote Sensing of Environment*, Vol. 111, pp. 493–518.

Lefsky, M.A., Hudak, A.T., Cohen, W.B., and Acker, S.A. 2005. Geographic variability in lidar predictions of forest stand structure in the Pacific Northwest. *Remote Sensing of Environment*, Vol. 95, No. 4, pp. 532–548.

Lentile, L.B., Smith, A.M.S., Hudak, A.T., Morgan, P., Bobbitt, M., Lewis, S.A., and Robichaud, P. 2009. Remote sensing for prediction of 1-year post-fire ecosystem condition. *International Journal of Wildland Fire*, Vol. 18, pp. 594–608.

Lieffers, V.J., Messier, C., Stadt, K.J., Gendron, F., and Comeau, P.G. 1999. Predicting and managing light in the understory of boreal forests. *Canadian Journal of Forest Research*, Vol. 29, pp. 796–811.

Lovell, J.L., Jupp, D.L.B., Culvenor, D.S., and Coops, N.C. 2003. Using airborne and ground-based ranging lidar to measure canopy structure in Australian forests. *Canadian Journal of Remote Sensing*, Vol. 29, No. 5, pp. 607–622.

Magnussen, S., and Boudewyn, P. 1998. Derivations of stand heights from airborne laser scanner data with canopy-based quantile estimators. *Canadian Journal of Forest Research*, Vol. 28, No. 7, pp. 1016–1031.

Means, J.E., Acker, S.A., Harding, D.J., Blair, J.B., Lefsky, M.A., Cohen, W.B., Harmon, M.E., and McKee, W.A. 1999. Use of large-footprint scanning airborne lidar to estimate forest stand characteristics in the Western Cascades of Oregon. *Remote Sensing of Environment*, Vol. 67, pp. 298–308.

Morsdorf, F., Kotz, B., Meier, E., Itten, K.I., and Allgower, B. 2006. Estimation of LAI and fractional cover from small footprint airborne laser scanning data based on gap fraction. *Remote Sensing of Environment*, Vol. 104, No. 1, pp. 50–61.

Pocewicz, A., Gessler, P.E., and Robinson, A.P. 2004. The relationship between leaf area index and Landsat spectral response across elevation, solar insolation, and spatial scales in a northern Idaho forest. *Canadian Journal Forest Research*, Vol. 34, pp. 465–480.

Pu, R., Xu, B., and Gong, P. 2003. Oakwood crown closure estimation by unmixing Landsat TM data. *International Journal of Remote Sensing*, Vol. 24, No. 22, pp. 4433–4445.

Riano, D., Valladares, F., Condes, S., and Chuvieco, E. 2004a. Estimation of leaf area index and covered ground from airborne laser scanner (Lidar) in two contrasting forests. *Agriculture and Forest Meteorology*, Vol. 124, pp. 269–275.

Riano, D., Chuvieco, E., Condes, S., Gonzales-Matesanz, J., and Ustin, S.L. 2004b. Generation of crown bulk density for *Pinus sylvestris* L. from lidar. *Remote Sensing of Environment*, Vol. 92, pp. 345–352.

Robinson, A.P., and Froese, R.E. 2004. Model validation using equivalence tests. *Ecological Modeling*, Vol. 176, pp. 349–358.

Robinson, A.P., Duursma, R.A., and Marshall, J.D. 2005. A regression-based equivalence test for model validation: shifting the burden of proof. *Tree Physiology*, Vol. 25, pp. 903–913.

Rowan, L.C., and Mars, J.C. 2003. Lithologic mapping in the Mountain Pass, California, area using Advanced Spaceborne Thermal Emission and Reflectance Radiometer (ASTER) data. *Remote Sensing of Environment*, Vol. 84, pp. 350–366.

Settle, J.J., and Drake, N.A. 1993. Linear mixing and the estimation of ground cover proportions. *International Journal of Remote Sensing*, Vol. 14, No. 6, pp. 1159–1177.

Shimabukuro, Y.E., and Smith, J.A. 1991. The least-squares mixing models to generate fraction images derived from remote-sensing multispectral data. *IEEE Transactions on Geoscience and Remote Sensing*, Vol. 29, pp. 16–20.

Smith, M.O., Johnson, P.E., and Adams, J.B. 1985. Quantitative determination of mineral types and abundances from reflectance spectra using principal components analysis. *Journal of Geophysical Research*, Vol. 90, pp. C797–C804.

Smith, A.M.S., Lentile, L.B., Hudak, A.T., and Morgan, P. 2007. Evaluation of linear spectral unmixing and dNBR for predicting post-fire recovery in a North American ponderosa pine forest. *International Journal of Remote Sensing*, Vol. 22, No. 20, pp. 5159–5166.

Smith, A.M.S., Strand, E.K., Steele, C.M., Hann, D.B., Garrity, S.R., Falkowski, M.J., and Evans, J.S. 2008. Production of vegetation spatial-structure maps by per-object analysis of juniper encroachment in multitemporal aerial photographs. *Canadian Journal of Remote Sensing*, Vol. 34, No. S2, pp. S268–S285.

Solberg, S., Næsset, E., Hanssen, K.H., and Christiansen, E. 2006. Mapping defoliation during a severe insect attack on Scots pine using airborne laser scanning. *Remote Sensing of Environment*, Vol. 102, pp. 364–376.

Sommers, B., Coold, K., Delalieax, S., Stuckens, J., Van der Zandle, D., Cerstaeten, W.W., and Coppin, P. 2009. Nonlinear hyperspectral mixture analysis for tree cover estimates in orchards. *Remote Sensing of Environment*, Vol. 113, pp. 1183–1193.

Strand, E., Smith, A.M.S., Bunting, S.C., Vierling, L.A., Hann, D.B., and Gessler, P.E. 2006. Wavelet estimation of plant spatial patterns in multi-temporal aerial photography. *International Journal of Remote Sensing*, Vol. 27, No. 9–10, pp. 2049–2054.

Strand, E.K., Vierling, L.A., Smith, A.M.S., and Bunting, S.C. 2008. Net changes in above ground woody carbon stock in western juniper woodlands, 1946–1998. *Journal of Geophysical Research — Biogeosciences*, Vol. 113, G01013. doi:10.1029/2007JG000544.

Theseira, M.A., Thomas, G., Taylor, J.C., Gemmell, F., and Varjo, J. 2003. Sensitivity of mixture modelling to end-member selection. *International Journal of Remote Sensing*, Vol. 24, No. 7, pp. 1559–1575

Thomas, V., Treitz, P., McCaughey, J.H., and Morrison, I. 2006. Mapping stand-level forest biophysical variables for a mixedwood boreal forest using lidar: an examination of scanning density. *Canadian Journal of Forest Research*, Vol. 36, pp. 34–47.

Thome, K.J., Biggar, S.F., and Slater, P.N. 2001. Effects of assumed solar spectral irradiance on intercomparisons of Earth-observing sensors. In *Sensors, Systems, and Next-Generation Satellites V*, 18 September 2001, Toulouse, France. Edited by H. Fujisada, J.B. Lurie, and K. Weber. Proceedings of SPIE, Volume 4540, The International Society for Optical Engineering, Bellingham, Wash. pp. 260–269.

Wellek, S. 2003. *Testing statistical hypotheses of equivalence*. Chapman & Hall, London, UK.

Xu, B., Gong, P., and Pu, R. 2003. Crown closure estimation of oak savannahs in a dry season with Landsat TM imagery: comparison of various indices through correlation analysis. *International Journal of Remote Sensing*, Vol. 24, No. 9, pp. 1811–1822.

Yuksel, A., Akay, A.E., and Gundogan, R. 2008. Using ASTER imagery in land use/cover classification of Eastern Mediterranean landscapes according to CORINE land cover project. *Sensors*, Vol. 8, No. 2, pp. 1237–1251.